# Three-Dimensional Nitrogen-Doped Carbonaceous Networks Anchored with Cobalt as Separator Modification Layers for Low-Polarization and Long-Lifespan Aluminum–Sulfur Batteries

Cheng Xu, Maider Zarrabeitia, Yueliang Li, Johannes Biskupek, Ute Kaiser, Xu Liu,* and Stefano Passerini*

**ABSTRACT:** Aluminum–sulfur (Al–S) batteries have attracted extensive interest due to their high theoretical energy density, inherent safety, and low cost. However, severe polarization and poor cycling performance significantly limit the development of Al–S batteries. Herein, three-dimensional (3D) nitrogen-doped carbonaceous networks anchored with cobalt ($Co@C_{Mel\text{-}ZIF}$) is proposed as a separator modification layer to mitigate these issues, prepared via carbonizations of a mixture of ZIF-7, melamine, and $CoCl_2$. It exhibits a 3D network structure with a moderate surface area and high average pore diameter, which is demonstrated to be effective in adsorbing the aluminum polysulfides and hindering the mobility of polysulfides across the separator for enhanced cyclic stability of Al–S batteries. Meanwhile, $Co@C_{Mel\text{-}ZIF}$ are characterized by abundant catalytic pyridinic-N and Co–$N_x$ active sites that effectively eliminate the barrier of sulfides' conversion and thereby facilitate the polarization reduction. As a result, Al–S cells based on the separator modified with $Co@C_{Mel\text{-}ZIF}$ exhibit a low voltage polarization of 0.47 V under the current density of 50 mA $g^{-1}$ at 20 °C and a high discharge specific capacity of 503 mAh $g^{-1}$ after 150 cycles. In contrast, the cell employing a bare separator exhibits a polarization of 1.01 V and a discharge capacity of 300 mAh $g^{-1}$ after 70 cycles under the same conditions. This work demonstrates that modifying the separators is a promising strategy to mitigate the high polarization and poor cyclability of Al–S batteries.

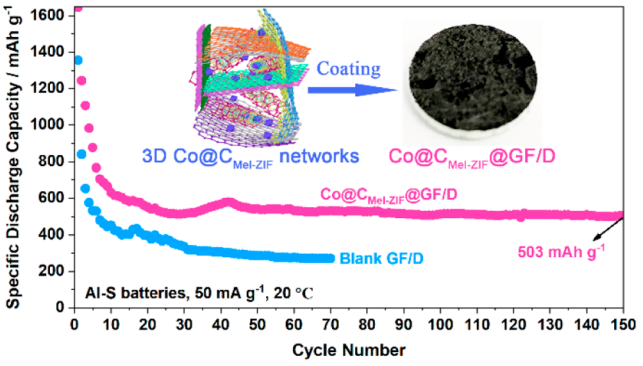


**KEYWORDS:** *aluminum sulfur batteries, MOFs, separators, catalysts, polarization, cyclability*

## INTRODUCTION

Al–S batteries are promising energy storage devices, because of the high theoretical capacity of the low-cost electrode materials (2980 mAh $g^{-1}$ and 8050 mAh $cm^{-3}$ for the Al anode; 1672 mAh $g^{-1}$ and 3459 mAh $cm^{-3}$ for the S cathode) and the inherent safety endowed by the nonflammable ionic liquid-based electrolytes.[1,2] Nonetheless, the conversion reaction of sulfur with $AlCl_4^-$ is rather sluggish, leading to severe cell polarization and, consequently, low energy density. Meanwhile, the notorious shuttle effect is also demonstrated in Al–S batteries, resulting in irreversible deposition of sulfide species on Al metal anodes and a severe decline in capacity.[3,4] Hence, mitigating the polarization and suppressing the shuttle effect are highly desired to improve the energy density and lifespan of Al–S batteries.

To date, extensive strategies have been developed to address these obstacles in Al–S batteries, including the design of sulfur hosts, electrolyte engineering, and separator modification.[5−9]

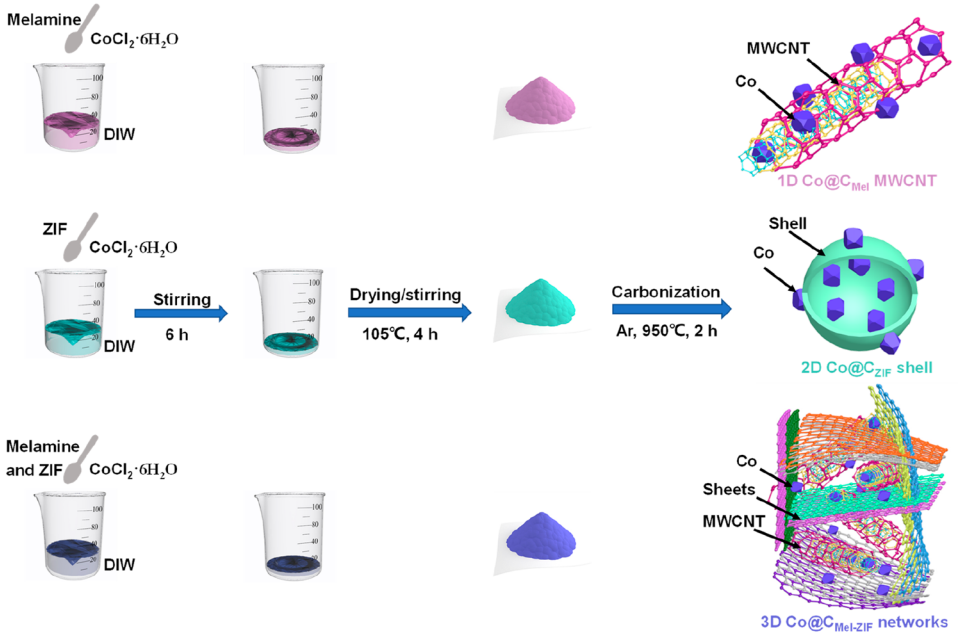


**Figure 1. Schematic of the synthesis method of Co@$C_{Mel}$, Co@$C_{ZIF}$, and Co@$C_{Mel-ZIF}$ samples.**

Various catalysts as sulfur hosts are proven to reduce the polarization of sulfur batteries, e.g., transition metal/sulfides,[10,11] single-atom catalysts,[12−15] nitrogen-doped carbon.[16] The cyclability of Al−S batteries is also enhanced with lithium salts employed as electrolyte additives, via promoting the chemical reactivation of aluminum polysulfides species.[17] Quasi-solid-state Al−S batteries employing cathode hosts with Co−$N_4$ as the catalytic sites facilitating Al−Cl and S−S bonds breakage exhibit effectively alleviated polarization, and the use of the quasi-solid electrolyte inhibiting the shuttle effect also improves the cyclic stability.[18] Furthermore, engineering of separator interface has been demonstrated to be an effective approach in mitigating the shuttle effect in metal−S batteries,[19−22] as the modification layer of separators can weaken the transport of polysulfides across the separator via physicochemical adsorption.[23] Previous researches have reported that carbonaceous nanomaterials with a high surface area and suitable pore size as the modification layer of separator can effectively enhance cyclic stability of the Al−S batteries by anchoring polysulfides during battery reaction.[24,25] When combined with nitrogen-based functional groups or transition-metal-based catalysts, the electrochemical reaction of the adsorbed polysulfide can be promoted, which leads to reduced polarization.[22] Importantly, considering the high viscosity of the most commonly used 1-ethyl-3-methyl-imidazolium chloride (EmimCl)-based electrolyte,[26] the separator modification materials with a favorable specific surface area and pore diameter are more inclined to promote electrolyte infiltration and to facilitate the adsorption of polysulfides. Therefore, the carbon materials as the absorbents of the polysulfides dissolved in electrolytes and the host of the catalysts require rational structure design.

Metal−organic frameworks (MOFs) have drawn significant interest due to their abundant structures, large surface area, and diverse pore size, which are also considered as the precursor to construct carbon nanomaterials for battery applications.[27] Nanoporous carbon materials with high surface area can be obtained through the carbonization of MOFs at high temperatures under an inert atmosphere for several hours.[28] Among them, ZIF-7-based MOF materials with imidazolate ligands rich in nitrogen are good candidates to yield N-doped porous carbons. Additionally, cobalt species present a significant catalytic effect for reducing the overpotential of Al−S batteries. Until now, the combination of ZIF-7-derived carbon materials and cobalt has received little attention in Al−S batteries.

Here, 3D nitrogen-doped carbonaceous networks anchored with cobalt (Co@$C_{Mel-ZIF}$) is proposed as a modifying layer of separator (Co@$C_{Mel-ZIF}$@GF/D) to mitigate the aforementioned issues of Al−S batteries, prepared via carbonizations of a mixture of ZIF-7, melamine, and $CoCl_2$. For comparison, the materials prepared via the carbonization of mixtures of $CoCl_2$ with either melamine or ZIF-7 were also prepared, namely, Co@$C_{Mel}$ and Co@$C_{ZIF}$, respectively. Among them, the Co@$C_{Mel-ZIF}$ sample presents a moderate surface area and a higher average pore diameter, exhibiting an effective a dsorption of polysulfides in the electrolyte and thereby limiting the shuttle effect for improved cyclability. Moreover, Co@$C_{Mel-ZIF}$ provides the most abundant N-related catalytic sites, effectively facilitating the reaction of the absorbed aluminum polysulfides, which results in low cell polarization. As a result, the Co@$C_{Mel-ZIF}$@GF/D-based Al−S batteries show a discharge specific capacity of 503 mAh $g^{-1}$ at the current density of 50 mA $g^{-1}$ after 150 cycles at 20 °C.

## RESULTS AND DISCUSSION

The carbon/cobalt composites were prepared via a simple one-step carbonization method, schematically shown in Figure 1. Cobalt chloride hexahydrate ($CoCl_2·6H_2O$), melamine, and/or ZIF-7 were dissolved in deionized water (DIW) to form homogeneous solutions. The solution was then dried at 110 °C in an oil bath under stirring. Subsequently, the resulting precursor was carbonized at 950 °C for 2 h under an Ar atmosphere, and the black carbon/cobalt composite powders were obtained. More details regarding the preparation can be found in the Experimental Section. The ZIF-7 used for the

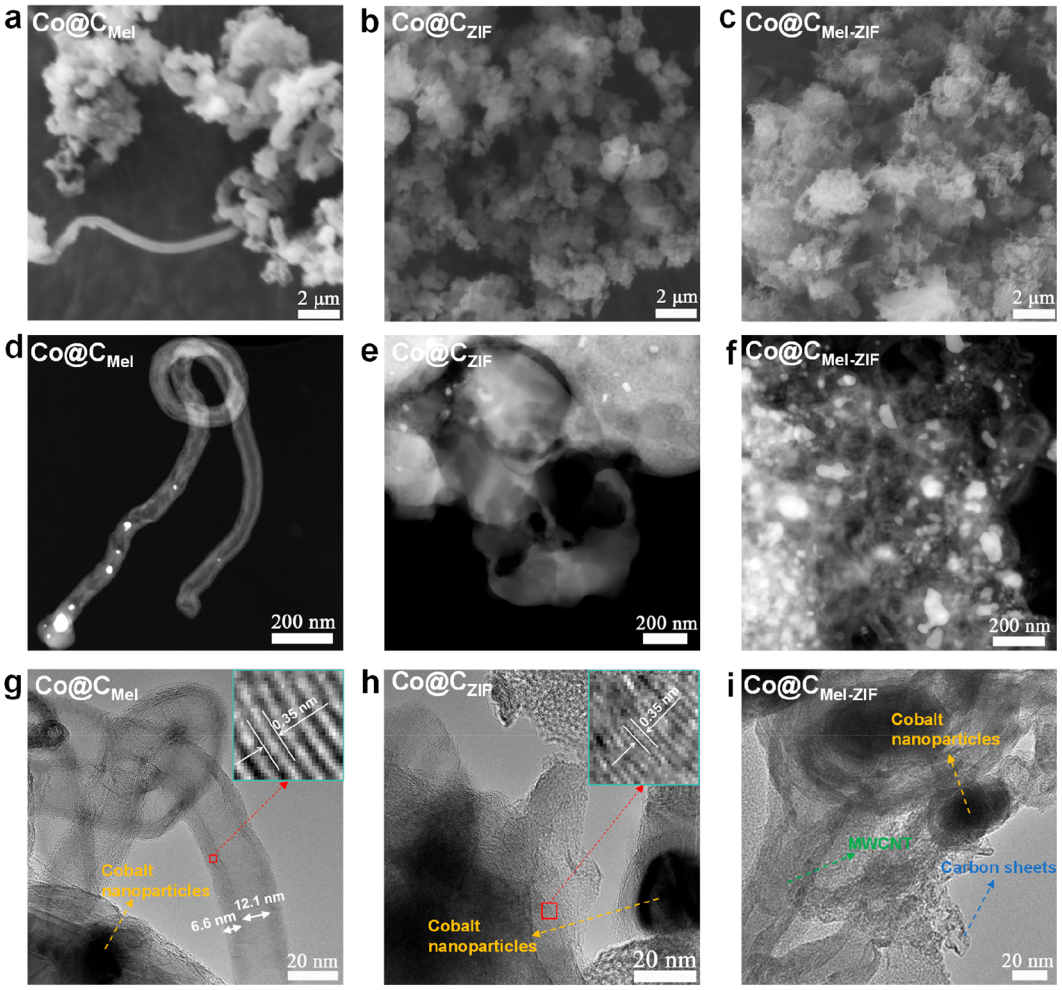


**Figure 2. (a–c) SEM, (d–f) HAADF, and (g–i) HRTEM images of (a, d, g) Co@C$_{Mel}$, (b, e, h) Co@C$_{ZIF}$, and (c, f, i) Co@C$_{Mel-ZIF}$ samples.**

preparation was synthesized via mixing $Zn(CH_3COO)_2{\cdot}2H_2O$ and benzimidazole in DIW, and the morphological as well as structural information on ZIF-7 are shown in Figure S1 in the Supporting Information.

The morphology of Co@C$_{Mel}$, Co@C$_{ZIF}$, and Co@C$_{Mel-ZIF}$ powders are visualized with scanning electron microscopy (SEM) and transmission electron microscopy (TEM), as shown in Figure 2. As depicted in Figure 2a, Co@C$_{Mel}$ contains a one-dimensional (1D) carbon tube and cobalt species. The high-angle annular dark-field (HAADF) image (see Figure 2d, as well as Figure S2a in the Supporting Information) reveals that the carbon tube is multi-walled carbon nanotubes with cobalt particles formed inside/around. Additionally, the HAADF image and the energy-dispersive X-ray spectroscopy (EDX) elemental mapping demonstrate that the cobalt particles outside the MWCNT exhibit severe aggregation (Figures S2a and S2b in the Supporting Information). As shown in Figure 2b, Co@C$_{ZIF}$ consists of 2D shell structures. From the HAADF image (Figure 2e) and the elemental mapping of this sample (Figure S2c,d), one can easily observe cobalt nanoparticles anchoring on the carbonaceous materials. The SEM (Figure 2c) and HAADF (Figure 2f) images demonstrate that Co@C$_{Mel-ZIF}$ shows 3D networks consisting of MWCNTs and carbon sheets (Figure 2c). EDX elemental mappings of C, O, N, and Co elements in Co@C$_{Mel}$, Co@C$_{ZIF}$ and Co@C$_{Mel-ZIF}$ are shown in Figures S2b, S2d, and S2f, respectively, in the Supporting Information. A uniform distribution of C, O, and N can be seen from all three samples, and smaller cobalt particles (represented by blue dots) tend to be generated in Co@C$_{ZIF}$ and Co@C$_{Mel-ZIF}$. Figure S3 in the Supporting Information shows the EDX spectra of the three powders, indicating that they are mainly composed of C, N, O, and Co.

Figures 2g–i show the HRTEM images of the three powders. As displayed in Figure 2g, Co@C$_{Mel}$ displays a MWCNT structure with an inner hole diameter and a wall thickness of ~12.1 and 6.6 nm, respectively. The interwall spacing of MWCNT is measured of ~0.35 nm, consistent with the reported work.[29] As shown in Figure 2h, the two-dimensional (2D) Co@C$_{ZIF}$ shell shows a crystal plane spacing of ~0.36 nm. In comparison to Co@C$_{Mel}$ and Co@C$_{ZIF}$, 3D Co@C$_{Mel-ZIF}$ exhibits the cross formation of MWCNT and carbon sheets, as shown in Figure 2i, as well as Figure S4 in the Supporting Information. Co@C$_{Mel-ZIF}$ presents more amorphous features compared to those of Co@C$_{Mel}$ and Co@C$_{ZIF}$. Besides, cobalt nanoparticles are encapsulated by carbon layers in three powders. Above TEM analyses presented above demonstrate that Co@C$_{Mel-ZIF}$ has a 3D structure (containing cross formation of MWCNT and carbon sheets).

The Ar adsorption–desorption isotherms of Co@C$_{Mel}$, Co@C$_{ZIF}$, and Co@C$_{Mel-ZIF}$ powders are compared in Figure S5 in the Supporting Information. The Brunauer–Emmett–

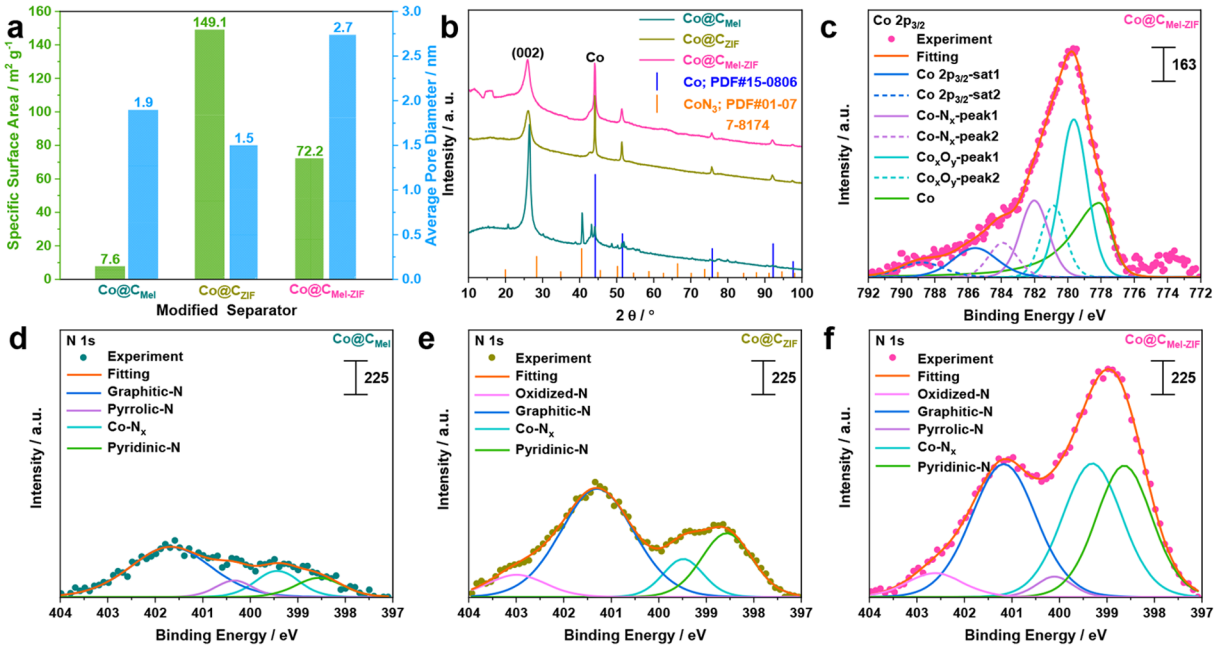


**Figure 3.** (a) Specific surface area and average pore diameter values, and (b) XRD patterns of $Co@C_{Mel}$, $Co@C_{ZIF}$, and $Co@C_{Mel\text{-}ZIF}$ powders. (c) Co $2p_{3/2}$ XPS spectrum of $Co@C_{Mel\text{-}ZIF}$. N 1s XPS spectra of (d) $Co@C_{Mel}$, (e) $Co@C_{ZIF}$, and (f) $Co@C_{Mel\text{-}ZIF}$.

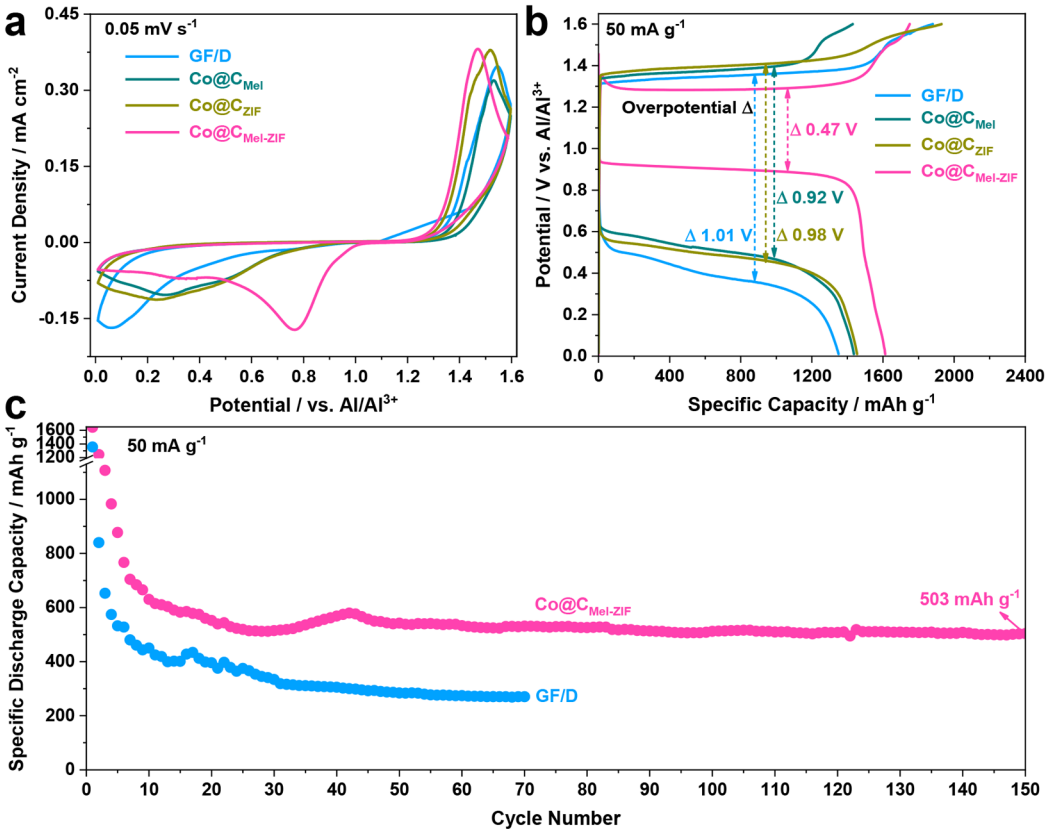


**Figure 4.** (a) CV curves at 0.05 mV $s^{-1}$ and (b) discharge/charge profiles at 50 mA $g^{-1}$ of Al–S cells with GF/D, $Co@C_{Mel}$, $Co@C_{ZIF}$, and $Co@C_{Mel\text{-}ZIF}$ modified GF/D separator from 0.01 to 1.6 V vs. $Al/Al^{3+}$. (c) Evolution of the specific discharge capacity of the GF/D and $Co@C_{Mel\text{-}ZIF}$@GF/D based cells upon long-term cycling at the current density of 50 mA $g^{-1}$.

Teller (BET) specific surface area and average pore size of the three powders are summarized in Figure 3a. $Co@C_{ZIF}$ presents the highest specific surface area of 149.1 $m^2$ $g^{-1}$, compared with those of $Co@C_{Mel}$ (7.6 $m^2$ $g^{-1}$) and $Co@C_{Mel\text{-}ZIF}$ (72.2 $m^2$ $g^{-1}$). This indicates that the carbonization of ZIF-7 leads to a superior surface area and is a suitable approach to produce

carbon host for catalysts. Co@$C_{Mel-ZIF}$ presents the largest average pore diameter of 2.7 nm with respect to Co@$C_{Mel}$ (1.9 nm) and Co@$C_{ZIF}$ (1.5 nm), which facilitates the contact of viscous electrolytes with the surface of the materials for more efficient adsorption of aluminum polysulfides.

The crystal structures of Co@$C_{Mel}$, Co@$C_{ZIF}$, and Co@$C_{Mel-ZIF}$ powders are characterized by XRD, as shown in Figure 3b. The sharp feature at 26.0° is observed from all the patterns and can be attributed to the (002) plane of crystalline carbon, e.g., graphite and CNTs. Co@$C_{Mel}$ additionally exhibits a feature at 40.7°, which originates from the generated $CoN_3$ (PDF No. 01-077-8174). The features at 44.2°, 51.5°, 75.8°, and 92.3° are ascribed to the cobalt metal (PDF No. 15-0806). Their intensity and sharpness indicate high crystallinity.

The surface chemical composition and valence states of Co@$C_{Mel}$, Co@$C_{ZIF}$, and Co@$C_{Mel-ZIF}$ powders are further investigated by X-ray photoelectron spectroscopy (XPS). As shown in Figure S6, Co@$C_{Mel-ZIF}$ displays a typical Co 2p signal.[30] Figure 3c presents the fitting results of Co $2p_{3/2}$ from Co@$C_{Mel-ZIF}$. The main peaks located at 778.1, 779.6, and 782.0 eV correspond to Co metal, $Co_xO_y$, and Co−$N_x$, respectively.[31] The cobalt content of these three samples was measured to be similar, according to the results of thermal gravimetric analysis (TGA) in the temperature range of 30−600 °C under an $O_2$ atmosphere (Figure S7 in the Supporting Information). N 1s XPS spectra of the three powders are summarized in Figures 3d−f. The peaks at 398.6, 399.3, 400.10, 401.2, and 402.6 eV are ascribed to pyridinic-N, Co−$N_x$, pyrrolic-N, graphitic-N, and oxidized-N species, respectively.[32,33] These species are observed from all studied samples except for Co@$C_{Mel}$, which does not contain oxidized-N and Co@$C_{ZIF}$ pyrrolic-N species. Nonetheless, their concentrations are different. Significantly, Co@$C_{Mel-ZIF}$ presents the strongest N signal and high pyridinic-N and Co−$N_x$ species contents. Apart from the oxidized-N, the other species have been demonstrated to exhibit strong catalytic effects, particularly the pyridinic-N and Co−$N_x$ species, for the breaking of Al−Cl and S−S bonds.[18,31,32] In the C 1s spectra shown in Figure S8 in the Supporting Information, −C−C−/−C═C−, −C−O−C−, −C═N, and −O−C═O/$\pi$−$\pi$ species are observed from all three samples. Therefore, a catalyzed electrochemical reaction and reduced cell voltage are expected for Co@$C_{Mel-ZIF}$ with a large number of catalytic sites.

To evaluate the electrochemical performance of Co@$C_{Mel}$, Co@$C_{ZIF}$, and Co@$C_{Mel-ZIF}$, GF/D separators modified with these materials were prepared, namely, Co@$C_{Mel}$@GF/D, Co@$C_{ZIF}$@GF/D, and Co@$C_{Mel-ZIF}$@GF/D, respectively. Figure S9 in the Supporting Information shows a photograph of a Co@$C_{Mel-ZIF}$@GF/D separator. The sulfur content of the S/graphene composite was calculated to be 54% by TGA, as shown in Figure S10 in the Supporting Information. With these separators, three-electrode T-shaped Al−S cells employing S/graphene electrodes as working electrodes, Al metal foil as counter and reference electrodes, and a mixture of aluminum chloride and EmimCl with a molar ratio of 1.3:1 (AE) as electrolytes (Figure S11 in the Supporting Information) were assembled and tested at 20 °C. Detailed information is shown in the Experimental Section.

Figure 4a illustrates the cyclic voltammetry (CV) curves of Al−S cells with different separators at a scan rate of 0.05 mV $s^{-1}$ from 0.01 to 1.6 V vs $Al/Al^{3+}$. When Co@$C_{Mel-ZIF}$@GF/D was employed, a pair of redox peaks with a cathodic peak at 0.52−0.98 V and anodic peak at 1.32−1.60 V was obtained, which shows much lower polarization than that for Co@$C_{Mel}$@GF/D and Co@$C_{ZIF}$@GF/D. Furthermore, reduced polarization was also observed in the discharge/charge profiles at a specific current of 50 mA $g^{-1}$, as displayed in Figure 4b. Co@$C_{Mel-ZIF}$@GF/D leads to the lowest average overpotential of 0.47 V, indicating the promoted reaction kinetics with the presence of the Co@$C_{Mel-ZIF}$ modification layer. The 3D Co@$C_{Mel-ZIF}$ networks provide intimate contact between catalysts and the polysulfides dissolved in the electrolyte and/or absorbed on the surface of the modification layer, reducing the barrier of their conversion reaction. To verify the origin of the capacity, Al metal batteries employing sulfur-free graphene cathodes and modified separators were assembled and tested at 20 °C. As shown in Figure S12 in the Supporting Information, their discharge specific capacities are lower than 13 mAh $g^{-1}$ at 50 mA $g^{-1}$, demonstrating that the capacity contribution of Al−S cells primarily originates from sulfur.

Figure 4c exhibits the evolution of the specific discharge capacity of Al−S batteries employing either GF/D or Co@$C_{Mel-ZIF}$@GF/D as a separator upon long-term cycling at 50 mA $g^{-1}$. Compared to the initial discharge specific capacity of 1351 mAh $g^{-1}$ reached with the GF/D separator, a higher specific capacity of 1613 mAh $g^{-1}$ was recorded when Co@$C_{Mel-ZIF}$@GF/D was employed as the separator. After 70 cycles, the Co@$C_{Mel-ZIF}$@GF/D-based cell maintained a lower polarization and higher specific discharge capacity of 512 mAh $g^{-1}$, which is superior to the GF/D-based cell exhibiting a specific capacity of 270 mAh $g^{-1}$ (Figure S13a in the Supporting Information). Moreover, even after 150 cycles, the Co@$C_{Mel-ZIF}$-based cell still presented a high discharge specific capacity of 503 mAh $g^{-1}$ (Figure S13b in the Supporting Information). These results imply that the 3D Co@$C_{Mel-ZIF}$ network modification layer could effectively limit the shuttle effect of aluminum polysulfide for improving the cyclic stability of Al−S batteries. Nonetheless, some dissolved polysulfide are still formed, which become no longer available for the reversible oxidation at cathode leading to the initial capacity drop.[8] Additionally, the cyclic ability of Al−S cells employing Co@$C_{Mel}$@GF/D and Co@$C_{ZIF}$@GF/D as the separators were also assembled and evaluated, exhibiting a slight improvement compared with that of the GF/D-based cell (see Figures S14 and S15 in the Supporting Information).

Furthermore, electrochemical impedance spectroscopy (EIS) was conducted toward the Al−S cells employing either GF/D or Co@$C_{Mel-ZIF}$@GF/D. As shown in Figure S16 in the Supporting Information, Co@$C_{Mel-ZIF}$@GF/D greatly alleviates the semicircle compared with that of GF/D, which demonstrates the effectively improved charge transfer ability of species leading to better electrochemical kinetics.[34]

To further investigate the mechanism for the reduced polarization, cobalt-free $C_{Mel-ZIF}$ was also prepared as a modification layer of the GFD separators ($C_{Mel-ZIF}$@GF/D). As shown in Figure S17 in the Supporting Information, $C_{Mel-ZIF}$ displays an amorphous carbon structure in agreement with the analysis in Figure 2i. Besides, $C_{Mel-ZIF}$ exhibits a high specific surface area of 480.8 $m^2$ $g^{-1}$, which is higher than that of Co@$C_{Mel-ZIF}$ (Figure S18 in the Supporting Information). The discharge/charge profiles of Al−S cells employing GF/D, $C_{Mel-ZIF}$@GF/D, or Co@$C_{Mel-ZIF}$@GF/D as separators are compared in Figure S19 in the Supporting Information. GF/D-based Al−S cells present severe polarization of 1.01 V, whereas Co@$C_{ZIF}$@GF/D and Co@$C_{Mel-ZIF}$@GF/D show a lower overpotential of 0.78 and 0.47 V, respectively. This

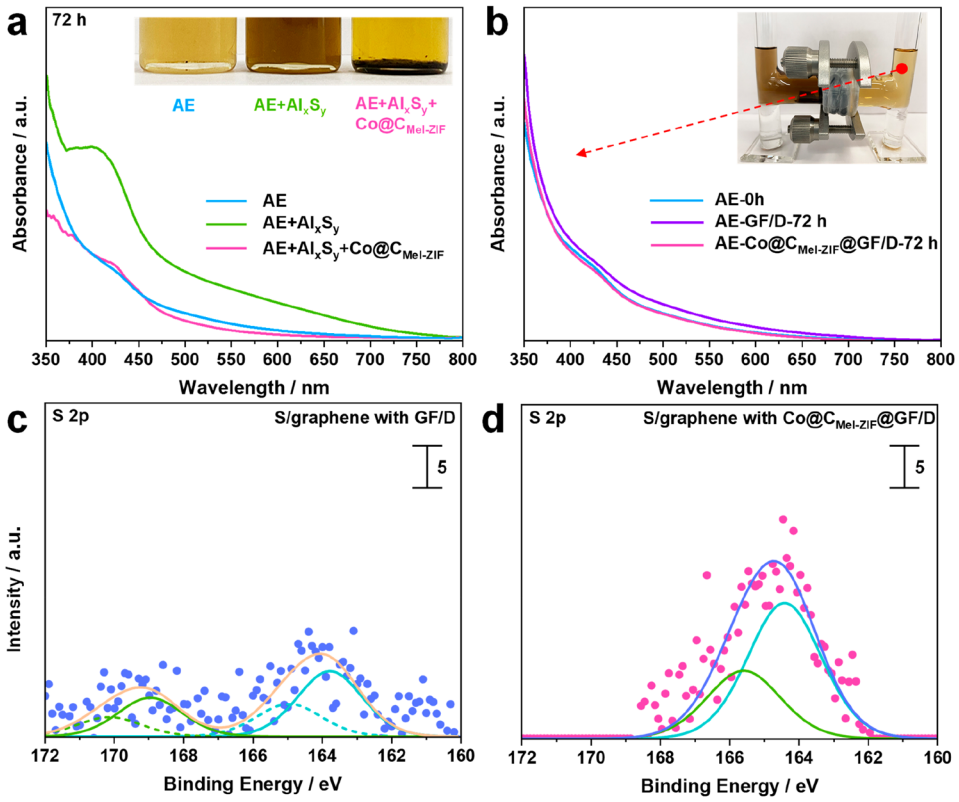


**Figure 5. (a) UV−vis spectra of blank AE electrolyte, AE electrolyte dissolved with polysulfide, and after adsorption with Co@C$_{Mel-ZIF}$ powders for 72 h. The inset shows the picture of the solutions. (b) UV−vis spectra of the blank AE electrolyte and the upper solution in the right tube of H-type cell employing GF/D and Co@C$_{Mel-ZIF}$@GF/D after a permeating test for 72 h. S 2p XPS spectra of S/graphene cathodes of Al−S cells were tested with (c) GF/D and (d) Co@C$_{Mel-ZIF}$@GF/D after 20 cycles.**

demonstrates that both the N-doped 3D carbonaceous host and the cobalt catalysts are important for the reduced polarization.

Table S1 in the Supporting Information compares the sulfur mass loading, average discharge voltage, and other performance results achieved in this work with previous literature, clearly showing that the Co@C$_{Mel-ZIF}$@GF/D-based Al−S cells achieve better electrochemical performance. To confirm the effectiveness of the Co@C$_{Mel-ZIF}$ layer, Al−S cells with a high sulfur mass loading (2 mg cm$^{-2}$) were assembled. As shown in Figure S20 in the Supporting Information, the Co@C$_{Mel-ZIF}$ modification layer leads to a higher specific discharge capacity and lower cell polarization, although the promotion effect is weakened with increased sulfur loading.

To evaluate the adsorption ability of Co@C$_{Mel-ZIF}$ toward aluminum polysulfides, adsorption measurements were conducted. The electrolyte containing polysulfide (AE + Al$_x$S$_y$) was prepared via running a beaker cell pairing an S/carbon black (C65) cathode and an Al anode in a glovebox for three days. The color of the electrolyte turned from initially light yellow to brown due to the dissolution of polysulfides, as shown in the inset of Figure 5a. The UV−vis spectra of AE + Al$_x$S$_y$ revealed a significant increase in adsorption in the region from 375 to 700 nm, which is unambiguously attributed to dissolved polysulfides. In a further step, 5 mg of Co@C$_{Mel-ZIF}$ powder was added into 2 mL of polysulfides-containing electrolyte. After 72 h, the brown solution turned back to light yellow (inset of Figure 5a), demonstrating the adsorption of the polysulfide by the Co@C$_{Mel-ZIF}$ powder. The removal of the polysulfides in the solution was also evidenced by decreased adsorption in the UV−vis spectra shown in Figure 5a. These results prove that Co@C$_{Mel-ZIF}$ possesses a stronger static adsorption capability toward Al$_x$S$_y$ species, indicating the possibility of suppressing the polysulfide shuttle between the cathodes and anodes.

Next, H-type cells (inset of Figure 5b) were employed to evaluate the hindrance of GF/D and Co@C$_{Mel-ZIF}$@GF/D toward the polysulfide shuttle. In the H-type cell, the left and right tubes were respectively filled with AE + Al$_x$S$_y$ and AE solutions with a GF/D or Co@C$_{Mel-ZIF}$@GF/D separator in between. After equilibration for 72 h, no obvious color difference was observed with the naked eye (Figure S21 in the Supporting Information), indicating that the permeation of polysulfides was not extensive for both of the separators. Following, the solution in the right tube of the H-type cells after standing 72 h was further characterized using UV−vis spectroscopy, as shown in Figure 5b. The solution taken from the GF/D equipped H-cell (AE-GF/D-72 h) showed higher adsorption with respect to the initial AE solution, while the solution from the Co@C$_{Mel-ZIF}$@GF/D H-cell (Co@C$_{Mel-ZIF}$@GF/D-72 h) is consistent with the fresh solution. This confirms that Co@C$_{Mel-ZIF}$ modified GF/D can limit the polysulfide diffusion.

To further verify the adsorption ability of Co@C$_{Mel-ZIF}$ on aluminum polysulfides in the Al−S batteries, the cycled S/graphene electrodes were collected from the cells and subjected to XPS characterization. Figure 5c,d displays the S 2p XPS spectra of the S/graphene cathodes in Al−S cells after

20 discharge/charge cycles with GF/D and Co@$C_{Mel\text{-}ZIF}$@GF/D separators, respectively. Obviously, the S/graphene cathode cycled with Co@$C_{Mel\text{-}ZIF}$@GF/D exhibits a stronger S 2p peak signal with regard to the one with GF/D, indicating that the Co@$C_{Mel\text{-}ZIF}$ layer effectively limits the irreversible shuttling of polysulfides from the cathode to the anode.

## CONCLUSION

Co@$C_{Mel}$, Co@$C_{ZIF}$, and Co@$C_{Mel\text{-}ZIF}$ prepared via carbonizing the mixture of $CoCl_2$ with melamine and/or ZIF-7 were employed to modify the separators for Al−S batteries. 3D Co@$C_{Mel\text{-}ZIF}$ possessing a moderate surface area and high average pore diameters, along with abundant pyridinic-N and Co−$N_x$ active sites, has been verified to be the optimal one. The large catalytic sites effectively reduced the polarization of the Al−S cells. Co@$C_{Mel\text{-}ZIF}$ powder exhibits verified adsorption ability toward the dissolved aluminum polysulfides, and Co@$C_{Mel\text{-}ZIF}$@GF/D provides a better physicochemical hindrance against the shuttle effect, with respect to the GF/D separator, which therefore promotes the cyclic stability of Al−S batteries. These results demonstrate that modifying the separators is a promising strategy to mitigate the high polarization and poor cyclability of the Al−S batteries.

## EXPERIMENTAL SECTION

**Preparation of ZIF-7.** 1.402 g of zinc acetate dihydrate ($Zn(CH_3COO)_2{\cdot}2H_2O$, ≥95%, Sigma−Aldrich) and 2.36 g of benzimidazole (≥95 %, Sigma−Aldrich) were dissolved separately in 150 mL of DIW, then stirred for 2 h to reach uniform solutions. Subsequently, the former solution was slowly added to the latter one with stirring, and a milky white mixture was observed after 3 h. The mixture was washed several times with DIW and ethanol until the pH was neutral. Finally, ZIF-7 was obtained after being dried at 60 °C for overnight.

**Preparation of Co@$C_{Mel}$, Co@$C_{ZIF}$, Co@$C_{Mel\text{-}ZIF}$, and $C_{Mel\text{-}ZIF}$.** Melamine (≥95 %, Sigma−Aldrich) was initially ground via ball milling at 800 rpm for 30 min. Next, 3 g of melamine and 0.0546 g of cobalt chloride hexahydrate ($CoCl_2{\cdot}6H_2O$, 99.9%, Thermo Scientific) were dissolved in 40 mL of DIW and stirred for 4 h. The mixture was then dried with an oil bath under stirring at 110 °C for 2 h to obtain the precursor (pink powder). Finally, the precursor was heated at 950 °C for 2 h with a heating rate of 5 °C $min^{-1}$ under an Ar atmosphere, and the black Co@$C_{Mel}$ powder was obtained.

Similarly, Co@$C_{ZIF}$ and Co@$C_{Mel\text{-}ZIF}$ were separately synthesized by following the synthesis method of Co@$C_{Mel}$. For Co@$C_{ZIF}$, 3 g of ZIF-7 and 0.0546 g of $CoCl_2{\cdot}6H_2O$ were added into 40 mL of DIW and stirred for 4 h. For Co@$C_{Mel\text{-}ZIF}$, 0.5 g of ZIF, 2.5 g of melamine, and 0.0546 g of $CoCl_2{\cdot}6H_2O$ were dissolved in 40 mL of DIW and stirred for 4 h. In addition, Co-free $C_{Mel\text{-}ZIF}$ was synthesized by mixing 0.5 g of ZIF-7 with 2.5 g of melamine in DIW. Following the drying and carbonization process, black Co@$C_{ZIF}$, Co@$C_{Mel\text{-}ZIF}$, and $C_{Mel\text{-}ZIF}$ powders were obtained.

**Preparation of the Modified GF/D Separator.** Glass fiber membranes (Whatman GF/D) were used as the blank separator, which was modified by casting a slurry on their surface. Specifically, Co@$C_{Mel}$, Co@$C_{ZIF}$, or Co@$C_{Mel\text{-}ZIF}$ was mixed with polyacrylonitrile (PAN, Mw ≈ 150 000, Sigma−Aldrich) in a weight ratio of 8:1 using DMF (analytical pure, VWR) as the solvent and stirred until homogeneous. Then, the slurry was coated on one side of GF/D. After being dried at 110 °C under vacuum for 10 h, discs with a diameter of 10 mm were cut and utilized as the separators. The mass loading of Co@$C_{Mel}$, Co@$C_{ZIF}$, and Co@$C_{Mel\text{-}ZIF}$ were 0.2 mg $cm^{-2}$.

**Characterization.** The morphology and structure of samples were characterized via SEM (Zeiss LEO 1550 microscope equipped with an EDX detector) and TEM (FEI Titan 80-330 with an image $C_s$-corrector operated at 80 kV, and Thermo Scientific Talos F200X with a windowless 4-quadrant EDX detector operated at 200 kV). The crystal structures were characterized with XRD (Bruker D8 Avance diffractometer, using Cu K$\alpha$ radiation) in a 2$\theta$ range of 10°−100°. The specific surface area and pore diameter of the samples were measured by Brunauer−Emmett−Teller (BET) (Autosorb-iQ, Quantachrome) at 87 K under the Ar absorption−desorption isotherms. The cobalt content of the samples and sulfur content were measured using thermogravimetric analysis (TGA) with a heating rate of 10 °C $min^{-1}$ from 30 to 600 °C under $O_2$ and $N_2$ atmospheres, respectively. The UV-vis spectra of the electrolytes were conducted with a Shimadzu Model 1800 UV-vis spectrometer). The surface chemical composition of pristine Co@$C_{Mel}$, Co@$C_{ZIF}$, and Co@$C_{Mel\text{-}ZIF}$ was investigated by means of X-ray photoelectron spectroscopy (XPS). The measurements were conducted using a monochromatic Al K$\alpha$ ($h\nu$ = 1.487 eV) X-ray source and a Phoibos 150 XPS spectrometer (SPECS-Surface concept) equipped with a microchannel plate and Delay Line Detector (DLD). The high-resolution scans were acquired with an X-ray power source of 200 W (15 kV), a pass energy of 30 eV, and 0.1 eV energy steps in a fixed analyzer transmission mode. CasaXPS software was used for fitting the spectra, using a nonlinear Shirley-type background and, in general, 70% Gaussian and 30% Lorentzian profile functions. The same experimental conditions were applied for the cycled separators (GF/D and Co@$C_{Mel\text{-}ZIF}$) and cycled S/graphene cathodes tested with different separators.

**Electrochemical Measurements.** Three-electrode, T-shaped cells employing S/graphene cathodes, with Al metal foils as the counter and reference electrodes, were assembled in an Ar-filled glovebox with $O_2$ and $H_2O$ levels of <0.1 ppm. S/graphene powder was prepared via a melt-diffusion method. 0.11 g of graphene (The Sixth Element, Inc.) and 0.5 g of sulfur (99.98%, Sigma−Aldrich) were mixed evenly and encapsulated in a glass tube and heated at 155 °C in a vacuum of $1 \times 10^{-1}$ mbar for 10 h. Afterward, S/graphene with a sulfur content of 54 wt % was obtained. Then, the DMF-based slurry made by mixing S/graphene, PAN and carbon black with a weight ratio of 70:15:15, was coated on the nongraphitic carbon paper (Osaka Gas Chemicals). After drying at 50 °C under vacuum for 5 h, discs with a diameter of 10 mm were cut and used as the cathode. The sulfur areal loading in the electrodes was 0.7 and 2 mg $cm^{-2}$, corresponding to 37.8% of the total electrode loading (1.85 and 5.29 mg $cm^{-2}$) and 34% of the total (electrode loading + separator coating) loading (2.05 and 5.49 mg $cm^{-2}$). The adsorption and catalysis of polysulfides are affected by the mass ratio between sulfur and modified layer. Al discs (99.99%, thickness of 100 $\mu$m) with a diameter of 10 mm, polished with sandpaper before use, were used as the counter and reference electrodes. 1-Ethyl-3-methylimidazolium chloride (EmimCl, > 98%, IoLiTec) mixed with $AlCl_3$ (≥99.99%, Alfa Aesar) in the 1:1.3 molar ratio was used as the electrolyte. The cycling performance and discharge/charge of Al−S batteries were investigated using a MACCOR series 4000 battery cycler at 20 °C. Cyclic voltammetry (CV) curves were tested via the galvanostat/potentiostat VMP2 (Bio-Logic, France).

**Permeation and Adsorption Test.** The electrolyte containing polysulfide was prepared by operating a beaker cell employing a S/C65 cathode and an Al anode in a glovebox. The mass loading of sulfur was 1.5 mg $cm^{-2}$, and the reaction area of the S/C65 cathode and Al anode was 6 $cm^2$. The beaker cell applied with 15 mL of electrolytes was cycled at the current of 400 $\mu$A for 3 days. A brown polysulfide-contained electrolyte (PSE) was obtained. For the permeation experiments with the H-type cell, 6 mL PSE and polysulfide-free electrolyte were separately added into both permeating tubes simultaneously. Between them, a separator (GF/D or Co@$C_{Mel\text{-}ZIF}$-modified GF/D) was used. After permeation for 3 days, the upper electrolytes from the right tube were extracted and characterized by UV-vis.

In the adsorption test, 5 mg of Co@$C_{Mel\text{-}ZIF}$ powders was added into 2 mL of PSE, and mixed evenly. After standing at room temperature for 3 days, the upper solution was characterized with UV-vis.

## AUTHOR INFORMATION


### Corresponding Authors

**Stefano Passerini** − *Helmholtz Institute Ulm (HIU), D-89081 Ulm, Germany; Karlsruhe Institute of Technology (KIT), D-76021 Karlsruhe, Germany; Chemistry Department, Sapienza University, I-00185 Rome, Italy;* orcid.org/0000-0002-6606-5304; Email: stefano.passerini@kit.edu

**Xu Liu** − *Helmholtz Institute Ulm (HIU), D-89081 Ulm, Germany; Karlsruhe Institute of Technology (KIT), D-76021 Karlsruhe, Germany;* orcid.org/0000-0003-0532-316X; Email: xu.liu@kit.edu

### Authors

**Cheng Xu** − *Helmholtz Institute Ulm (HIU), D-89081 Ulm, Germany; Karlsruhe Institute of Technology (KIT), D-76021 Karlsruhe, Germany*

**Maider Zarrabeitia** − *Helmholtz Institute Ulm (HIU), D-89081 Ulm, Germany; Karlsruhe Institute of Technology (KIT), D-76021 Karlsruhe, Germany*

**Yueliang Li** − *Helmholtz Institute Ulm (HIU), D-89081 Ulm, Germany; Karlsruhe Institute of Technology (KIT), D-76021 Karlsruhe, Germany; Electron Microscopy Group of Materials Science, Ulm University, D-89081 Ulm, Germany*

**Johannes Biskupek** − *Electron Microscopy Group of Materials Science, Ulm University, D-89081 Ulm, Germany*

**Ute Kaiser** − *Electron Microscopy Group of Materials Science, Ulm University, D-8 908 1 Ulm, Germany*


### Notes

The authors declare no competing financial interest.

## ACKNOWLEDGMENTS


This work was supported by the China Scholarship Council (CSC). All authors acknowledge the basic funding of the Helmholtz Association.


## REFERENCES


(1) Gao, T.; Li, X.; Wang, X.; Hu, J.; Han, F.; Fan, X.; Suo, L.; Pearse, A. J.; Lee, S. B.; Rubloff, G. W.; Gaskell, K. J.; Noked, M.; Wang, C. A Rechargeable Al/S Battery with an Ionic-Liquid Electrolyte. *Angew. Chem., Int. Ed.* **2016**, *55* (34), 9898−9901.

(2) Pang, Q.; Meng, J.; Gupta, S.; Hong, X.; Kwok, C. Y.; Zhao, J.; Jin, Y.; Xu, L.; Karahan, O.; Wang, Z.; Toll, S.; Mai, L.; Nazar, L. F.; Balasubramanian, M.; Narayanan, B.; Sadoway, D. R. Fast-Charging Aluminium-Chalcogen Batteries Resistant to Dendritic Shorting. *Nature* **2022**, *608* (7924), 704−711.

(3) Yu, X.; Manthiram, A. Ambient-Temperature Energy Storage with Polyvalent Metal-Sulfur Chemistry. *Small Methods* **2017**, *1* (11), 1700217.

(4) Jay, R.; Jadhav, A. L.; Gordon, L. W.; Messinger, R. J. Soluble Electrolyte-Coordinated Sulfide Species Revealed in Al-S Batteries by Nuclear Magnetic Resonance Spectroscopy. *Chem. Mater.* **2022**, *34*, 4486−4495.

(5) Zhou, Q.; Wu, Y.; Gautam, J.; Wang, D.; Jiang, X.; Ma, Z.; Zhang, H.; Ni, L.; Diao, G. The Current State of Electrolytes and Cathode Materials Development in the Quest for Aluminum-Sulfur Batteries. *Coord. Chem. Rev.* **2023**, *474*, 214856.

(6) Li, H.; Lampkin, J.; Garcia-araez, N. Facilitating Charge Reactions in Al-S Batteries with Redox Mediators. *ChemSusChem* **2021**, *14*, 3139−3146.

(7) Sungjemmenla; Soni, C. B.; Kumar, V. Recent Advances in Cathode Engineering to Enable Reversible Room-Temperature Aluminium-Sulfur Batteries. *Nanoscale Adv.* **2021**, *3* (6), 1569−1581.

(8) Xu, C.; Diemant, T.; Liu, X.; Passerini, S. Modified Solid Electrolyte Interphases with Alkali Chloride Additives for Aluminum-Sulfur Batteries with Enhanced Cyclability. *Adv. Funct. Mater.* **2023**, *33*, 2214405.

(9) Yang, H.; Yin, L.; Liang, J.; Sun, Z.; Wang, Y.; Li, H.; He, K.; Ma, L.; Peng, Z.; Qiu, S.; Sun, C.; Cheng, H.-M.; Li, F. An Aluminum-Sulfur Battery with a Fast Kinetic Response. *Angew. Chem.* **2018**, *130* (7), 1916−1920.

(10) Xu, H.; Bai, T.; Chen, H.; Guo, F.; Xi, J.; Huang, T.; Cai, S.; Chu, X.; Ling, J.; Gao, W.; Xu, Z.; Gao, C. Low-Cost AlCl3/Et3NHCl Electrolyte for High-Performance Aluminum-Ion Battery. *Energy Storage Mater.* **2019**, *17*, 38−45.

(11) Lin, Z.; Mao, M.; Lv, T.; Li, S.; Hu, Y.; Li, H.; Huang, X.; Chen, L.; Suo, L. Electroactive-Catalytic Conductive Framework for Aluminum-Sulfur Batteries. *Energy Storage Mater.* **2022**, *51* (July), 266−272.

(12) Ju, S.; Yuan, C.; Zheng, J.; Yao, L.; Zhang, T.; Xia, G.; Yu, X. Identifying Single-Atom Catalysts for Boosted Al-S Conversion Reactions. *Energy Storage Mater.* **2022**, *52*, 524−533.

(13) Wang, Z.; Zheng, X.; Chen, A.; Han, Y.; Wei, L.; Li, J. Unraveling the Anchoring E Ff Ect of MXene- Supported Single Atoms as Cathodes for Aluminum - Sulfur Batteries. *ACS Mater. Lett.* **2022**, *4*, 1436−1445.

(14) Zhang, Y.; Liu, S.; Ji, Y.; Ma, J.; Yu, H. Emerging Nonaqueous Aluminum-Ion Batteries: Challenges, Status, and Perspectives. *Adv. Mater.* **2018**, *30* (38), 1706310.

(15) Zhang, J.; He, R.; Jia, L.; You, C.; Zhang, Y.; Liu, M.; Tian, N.; Lin, H.; Wang, J. Strategies for Realizing Rechargeable High Volumetric Energy Density Conversion-Based Aluminum-Sulfur Batteries. *Adv. Funct. Mater.* **2023**, *33*, 2305674.

(16) Ju, S.; Ye, J.; Zhang, H.; Wang, W.; Xia, G.; Cui, W.; Yang, Y.; Pan, H.; Yu, X. Recognizing the Contrasting Role of N, O Dual-Coordinated Single-Atom Iron Catalyst in Li-S and Al-S Batteries. *Energy Storage Mater.* **2023**, *56*, 1−12.

(17) Yu, X.; Boyer, M. J.; Hwang, G. S.; Manthiram, A. Room-Temperature Aluminum-Sulfur Batteries with a Lithium-Ion-Mediated Ionic Liquid Electrolyte. *Chem* **2018**, *4* (3), 586−598.

(18) Huang, Z.; Wang, W.; Song, W. L.; Wang, M.; Chen, H.; Jiao, S.; Fang, D. Electrocatalysis for Continuous Multi-Step Reactions in Quasi-Solid-State Electrolytes Towards High-Energy and Long-Life Aluminum-Sulfur Batteries. *Angew. Chem., Int. Ed.* **2022**, *61* (2), No. e202202696.

(19) Yu, X.; Manthiram, A. Electrochemical Energy Storage with a Reversible Nonaqueous Room-Temperature Aluminum-Sulfur Chemistry. *Adv. Energy Mater.* **2017**, *7* (18), 1700561.

(20) Li, Z.; Zhou, S.; Wu, X.; Zhang, B.; Yu, X.; Pei, F.; Liao, H. G.; Qiao, Y.; Zhou, H.; Sun, S. G. Restraining Shuttle Effect in Rechargeable Batteries by Multifunctional Zeolite Coated Separator. *Adv. Funct. Mater.* **2023**, *33* (8), 2211774.

(21) Yang, Y.; Fu, W.; Zhang, D.; Ren, W.; Zhang, S.; Yan, Y.; Zhang, Y.; Lee, S. J.; Lee, J. S.; Ma, Z. F.; Yang, J.; Wang, J.; Nuli, Y. Toward High-Performance Mg-S Batteries via a Copper Phosphide Modified Separator. *ACS Nano* **2023**, *17* (2), 1255−1267.

(22) Wang, F.; Jiang, M.; Zhao, T.; Meng, P.; Ren, J.; Yang, Z.; Zhang, J.; Fu, C.; Sun, B. Atomically Dispersed Iron Active Sites

Promoting Reversible Redox Kinetics and Suppressing Shuttle Effect in Aluminum-Sulfur Batteries. *Nano-Micro Lett.* **2022**, *14* (1), 169.
(23) Hao, H.; Hutter, T.; Boyce, B. L.; Watt, J.; Liu, P.; Mitlin, D. Review of Multifunctional Separators: Stabilizing the Cathode and the Anode for Alkali (Li, Na, and K) Metal-Sulfur and Selenium Batteries. *Chem. Rev.* **2022**, *122* (9), 8053−8125.
(24) Banerjee, S.; Han, X.; Siegler, M. A.; Miller, E. M.; Bedford, N. M.; Bukowski, B. C.; Thoi, V. S. Flexible 2D Boron Imidazolate Framework for Polysulfide Adsorption in Lithium-Sulfur Batteries. *Chem. Mater.* **2022**, *34* (23), 10451−10458.
(25) Wang, C.; Huang, J.; Cao, L.; Li, J.; He, C.; Li, H.; Tian, J.; Kajiyoshi, K. Intrinsic Defects Promote Rapid Conversion of Polysulfides on Carbon Surface to Achieve High Rate Performance. *Carbon, N.Y.* **2021**, *183*, 899−911.
(26) Xu, B.; Qu, R.; Ling, G. Anodic Behavior of Mg in Acidic AlCl3−1-Ethyl-3-Methyl-Imidazolium Chloride Ionic Liquid. *Electrochim. Acta* **2014**, *149*, 300−305.
(27) Wang, L.; Wang, Z.; Xie, L.; Zhu, L.; Cao, X. ZIF-67-Derived N-Doped Co/C Nanocubes as High-Performance Anode Materials for Lithium-Ion Batteries. *ACS Appl. Mater. Interfaces* **2019**, *11* (18), 16619−16628.
(28) Hao, M.; Qiu, M.; Yang, H.; Hu, B.; Wang, X. Recent Advances on Preparation and Environmental Applications of MOF-Derived Carbons in Catalysis. *Sci. Total Environ.* **2021**, *760*, 143333.
(29) Kiang, C. H.; Endo, M.; Ajayan, P. M.; Dresselhaus, G.; Dresselhaus, M. S. Size Effects in Carbon Nanotubes. *Phys. Rev. Lett.* **1998**, *81* (9), 1869−1872.
(30) Wagner, C. D.; Riggs, W. M.; Davis, L. E.; Moulder, J. F.; Muilenberg, G. E. *Handbook of X-ray Photoelectron Spectroscopy*, First Edition; Perkin−Elmer Corporation Physical Electronic Division: Eden Prairie, MN, 1979; p 78.
(31) Chen, Y. Z.; Wang, C.; Wu, Z. Y.; Xiong, Y.; Xu, Q.; Yu, S. H.; Jiang, H. L. From Bimetallic Metal-Organic Framework to Porous Carbon: High Surface Area and Multicomponent Active Dopants for Excellent Electrocatalysis. *Adv. Mater.* **2015**, *27* (34), 5010−5016.
(32) Morozan, A.; Jégou, P.; Jousselme, B.; Palacin, S. Electrochemical Performance of Annealed Cobalt-Benzotriazole/CNTs Catalysts towards the Oxygen Reduction Reaction. *Phys. Chem. Chem. Phys.* **2011**, *13* (48), 21600−21607.
(33) Wang, T.; Kou, Z.; Mu, S.; Liu, J.; He, D.; Amiinu, I. S.; Meng, W.; Zhou, K.; Luo, Z.; Chaemchuen, S.; Verpoort, F. 2D Dual-Metal Zeolitic-Imidazolate-Framework-(ZIF)-Derived Bifunctional Air Electrodes with Ultrahigh Electrochemical Properties for Rechargeable Zinc-Air Batteries. *Adv. Funct. Mater.* **2018**, *28* (5), 1705048.
(34) Yang, B. Z.; Xie, P.; Luo, Q.; Li, Z. W.; Zhou, C. Y.; Yin, Y. H.; Liu, X. B.; Li, Y. S.; Wu, Z. P. Binder-Free $\omega$-$Li_3V_2O_5$ Catalytic Network with Multi-Polarization Centers Assists Lithium-Sulfur Batteries for Enhanced Kinetics Behavior. *Adv. Funct. Mater.* **2022**, *32* (8), 2110665.